Salpakari, Jyri; Lund, Peter

Optimal and rule-based control strategies for energy flexibility in buildings with PV

Published in:
Applied Energy

DOI:
10.1016/j.apenergy.2015.10.036

Published: 01/01/2016

Document Version
Peer-reviewed accepted author manuscript, also known as Final accepted manuscript or Post-print

Please cite the original version:
Salpakari, J., & Lund, P. (2016). Optimal and rule-based control strategies for energy flexibility in buildings with PV. *Applied Energy*, *161*, 425-436. https://doi.org/10.1016/j.apenergy.2015.10.036

Optimal and rule-based control strategies for energy flexibility in buildings with PV

Jyri Salpakari*, Peter Lund

New Energy Technologies Group, Department of Applied Physics, School of Science, Aalto University

P.O.Box 14100, FI-00076 AALTO (Espoo), Finland

* Corresponding author, tel. +358 50 433 1262, email: jyri.salpakari@aalto.fi

Abstract

PV installations in buildings can utilize different on-site flexibility resources to balance mismatch in electricity production and demand. This paper studies cost-optimal and rule-based control for buildings with PV, employing a heat pump, thermal and electrical storage and shiftable loads as flexibility sources to increase the value of PV for the prosumer. The cost-optimal control minimizes variable electricity cost employing market data on electricity price and optionally constrains grid feed-in to zero; the rule-based control aims at maximizing PV self-consumption. The flexibility strategies are combined into a simulation model to analyze different system configurations over a full year.

The applicability of the new model is demonstrated with a case study with empirical data from a real low-energy house in Southern Finland. Compared to inflexible reference control with a constant price for bought electricity, cost-optimal control employing hourly market price of electricity achieved 13–25% savings in the yearly electricity bill. Moreover, 8–88% decrease in electricity fed into the grid was obtained. The exact values depend on PV capacity and the flexibility options chosen. Limiting grid feed-in to zero led to less energy efficient control. The most effective flexibility measures in this case turned out to be thermal storage with a heat pump and a battery, whereas shiftable appliances showed only a marginal effect.

Keywords: photovoltaics, intelligent building, demand side management, prosumer, energy storage, system control

Highlights:

- A new model of a heat pump with storage, a battery and shiftable appliances.
- Both fixed and variable condensing modes of the heat pump.
- A case study with a Finnish low-energy house.
- Cost-optimal control decreased cost by 13–25% and grid feed-in by 8–88%.
- Heat pump with storage and a battery were more effective than shiftable appliances.

Nomenclature

Symbols

C	specific heat
Co	Courant number
E	energy
g	time-step cost
J	cost function
$\dot{m}$	mass flow
i	general integer step variable
k	time step
l	log of shiftable appliance runs
n	number
N	end of optimization horizon
P	power
r	number of started shiftable appliance runs
T	temperature, daily number of turnovers
u	control vector
u^*	cost-optimal control
U	overall heat transfer coefficient, set of feasible controls
w	external data vector
x	state vector
X	set of feasible states
ε	heat exchanger effectiveness
η	efficiency

π	electricity price
ρ	density

Abbreviations

AC	alternating current
CHP	combined heat and power
COP	coefficient of performance
DHW	domestic hot water
DC	direct current
DP	dynamic programming
DSM	demand side management
FIT	feed-in tariff
GSHP	ground-source heat pump
PV	photovoltaics
TES	thermal energy storage
VRE	variable renewable electricity

Subscripts

battery	battery
C, comp	compressor
Ca	Carnot
cons	consumption
const	constant
curtailed	curtailed
CW	cold water
E	earth
el	electricity
fixed	fixed
h	hour
H	hot
HE	heat exchanger
heater	heater

I	input
inverter	inverter
l	low
L	load
m	medium
min	minimum
max	maximum
net	net
O	outdoor
P	constant pressure
runs	runs
s	side
S	storage
SH	space heating
shift, shiftable	shiftable
syst	system
R	return
tb	top and bottom

1. Introduction

The penetration of photovoltaics (PV) is increasing rapidly worldwide, with a 26% increase of installed capacity to 177 GW from 2013 to 2014 [1], and the trend is expected to continue [2]. Residential, commercial or industrial buildings represent a major segment of the PV market, with a 66% share of total installed capacity in Europe in 2013 [3]. Unlike conventional electricity production, PV electricity production is variable and uncertain, therefore the increasing capacity brings an additional challenge to balancing the demand and supply of electricity [4–9].

Power system flexibility measures to balance PV production can be classified into flexible generation, storage, interconnections, and demand-side management (DSM) [4,9–14]. In addition, turning surplus PV into thermal energy for heating and/or cooling, possibly including thermal energy storage (TES), may offer significant additional flexibility [9,15–23]. Buildings with PV can provide on-site flexibility in all these classes except interconnections. The potential flexibility sources comprise flexible distributed generation (e.g. micro-CHP), electrical storage (e.g. batteries), shiftable and curtailable electrical loads, and thermal conversion in building heating and cooling, possibly coupled

with thermal storage. The focus of this paper is on thermal conversion including TES, electrical storage and DSM with controllable loads. Dispatchable local distributed generation (e.g. micro-CHP) is not included here as it would incur extra investments in local energy production and the need for fuels.

Local DSM, thermal conversion and storage in a building with a PV installation can benefit the whole energy system by balancing the variable and uncertain PV feed-in. They can also benefit the prosumer (electricity consumer and producer) through increased self-consumption as well as price-responsive consumption, PV feed-in and arbitrage with electrical storage. Maximizing self-consumption is naturally incentivized in markets without a feed-in-tariff (FIT), such as Finland, or with FIT lower than electricity retail price, such as Germany [24], as the price paid for electricity fed to the grid is always lower than the retail price. Moreover, e.g. Germany and Italy have set separate self-consumption incentives [24]. Limitation of active power feed-in to 70% of maximum power output has also been imposed as grid integration regulation in some regions in Germany with high PV penetration [24,25]. Self-consumption is a more energy-efficient way to adhere to this limit than curtailment.

This paper presents a model for studying cost-optimal and self-consumption maximizing rule-based control of energy flexibility in a building with PV. The included flexibility sources are a ground-source heat pump (GSHP) with an auxiliary electric resistance heater and a water tank TES, a battery, and shiftable loads, such as washing machines. The selected flexibility sources are interesting in light of GSHP proliferation for energy efficiency [26], low cost of water tank TES [27,28], and the decreasing trend in Li-ion battery cost [29]. Shiftable appliances allow for lossless load shifting with no investment to storage capacity and only a limited effect to the activities in the building [9]. The potential of these flexibility sources to lower the electricity costs of the prosumer and to balance the variable and uncertain PV feed-in to the grid can be studied with the model.

The three control modes studied in this paper correspond to different market roles. In rule-based control, the building acts as a consumer which actively tries to avoid selling PV electricity by maximizing self-consumption and sells only when this is unsuccessful; selling is prohibited altogether in cost-optimal control with grid feed-in constrained to zero. In contrast, the building takes an active prosumer role in cost-optimal control, taking advantage of market price changes in both buying and selling.

There is a substantial body of literature on DSM and storage in PV integration to buildings. Many studies optimize DSM or storage control with PV and present results over a short time horizon, e.g. 1 day or 1 week [30–36]. In this paper, however, a full year is simulated with a 1-h time step. While studies with a short time horizon demonstrate optimal control in a realistic optimization horizon, the effect of seasonal and inter-day variations in PV production, price and load on the presented results is limited. Hence, the long-term performance in actual application is not evaluated. The seasonal effects are especially pronounced in northern locations with PV production concentrated to summertime and space heating demand to wintertime, such as Finland where the case study in this paper is situated. Inter-day PV production variations due to varying cloud coverage are significant worldwide. Moreover, a full-year simulation is less sensitive to the initial conditions of the system, such as initial storage state-of-charge. Hence, studies on rule-based and optimal control with time horizon of a full year or at least several months are reviewed here, starting with rule-based control studies.

Cao et al. [37] studied thermal storage with electrically heated DHW storage and a battery for PV and micro-wind production matching. Charging the DHW storage was found technically and economically more effective than a battery to reduce annual mismatch. In [38] and [39], a heat pump with thermal energy storage (TES) and a battery is used to increase self-consumption and lower peak grid injection from a PV system. Ref. [40] presents TES setpoint controls to match heat pump operation with PV production. Widén et al. [41] studied electrical storage, load shifting and PV array orientation for load matching. Kootstra et al. [42] studied a partially degraded second life battery with a PV system. More studies on rule-based control with PV can be found e.g. in a recent review [43]. Our paper adds to these studies by combining thermal storage, battery and shiftable appliances to a single model. Moreover, the performance of the rule-based control is compared directly to the cost-optimal one.

As for the optimal control studies, Wang et al. [44] presented robust optimization of household appliance and water heater scheduling with uncertain PV production. Guo et al. [45] solved stochastic optimization problems of scheduling a battery and shiftable loads. Widén and Munkhammar [46,47] studied optimal scheduling of shiftable loads with rule-based control of battery storage for PV self-consumption. The potential without extensive battery storage was found limited. Masa-Bote et al. [48] also combined optimal scheduling of shiftable loads with rule-based battery control, reducing the uncertainty of energy exchange with the grid due to forecast error from 40% to 2%. Li and Danzer [49] and Schreiber and Hochloff [50] solved optimal control of a battery with PV, the latter with a

capacity-dependent tariff to incentivize grid-benefiting operation. Ref. [51] presents model predictive control of a battery and TES with a heat pump, however without a detailed enough account on the employed models and optimization methods required for reproducibility or judging research limitations.

The flexibility sources studied in this paper, namely a GSHP with TES, a battery and shiftable loads, have not been combined in a simulation model with PV in a building for cost-optimal and rule-based control over a full year previously. Both variable and fixed condensing operating modes of a GSHP are included to such a model for the first time here as well. Moreover, contrary to previous work on cost-optimal control of a GSHP and TES with PV in a building over a full year, actual contract prices based on the electricity spot market price are employed in this paper instead of hypothetical prices, and the models and methods are documented to such an extent that the research limitations are clear and the study could be reproduced. Overall, physical realism has been strived for in the model, e.g. the modeling of the GSHP and TES is based on fundamental energy balances with explicit temperature modeling avoiding violations of the second law of thermodynamics, and includes the effect of temperature on the COP of the heat pump explicitly.

To demonstrate the new model and to verify the benefits from the controls with the different flexibility options, a case study on a Finnish low-energy house is also presented in this paper. Annual optimal control in sequential 24-h horizons is studied along with rule-based control. Different combinations of the flexibility sources and dimensions of the PV system, TES and battery are evaluated. The effects of heating system temperature level and variable vs. fixed condensing mode of the heat pump are also included. The 24-h horizon is a realistic optimization horizon in terms of day-ahead electricity price and weather forecast availability.

2. System model

The system model includes the flexibility sources, namely a ground-source heat pump with an auxiliary electric resistance heater and thermal storage, a Li-ion battery and shiftable appliances, along with DHW storage and an electric DHW heater. Fig. 1 depicts the energy flows and controls in the model. The heating and electrical system models are described in the following sections. Overall, physical realism has been strived for in the model. Some simplifications have been necessary to allow for solving cost-optimal control:

- Battery aging is neglected.

- The water tank TES is modeled as fully mixed, resulting in conservative performance with a heat pump compared to a stratified TES.
- The shiftable appliances are modeled with a single average demand cycle.

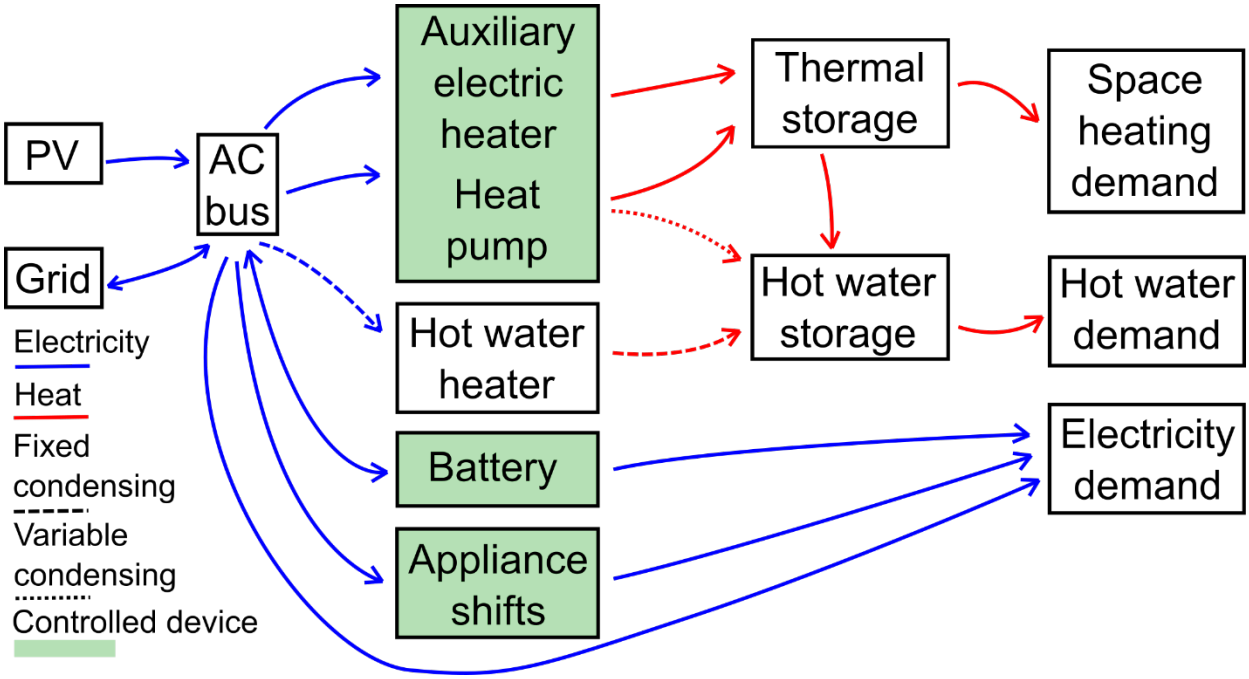

Figure 1. Energy flows and controls in the modeled system.

The model is designed for determining hourly energy balances: for mathematical tractability and to limit the computational burden in solving cost-optimal control over a full year, hourly data is used and control decisions are hourly. Even though solar radiation can vary abruptly and a sub-hourly time step is hence required for detailed grid interaction studies [52,53], the hourly time step is used for the following reasons:

- The time constant of hydronic radiators, used in the model as the heating system, is approximately 0.5 h [54]. Direct modeling of this dynamics is challenging as the heat transfer from radiators is affected by the geometry, surface temperatures and materials of the radiator and installation site, and the local air flow conditions that are affected by structures such as curtains and furniture [55]. Even if an idealized model was used for the radiator heat transfer, the situation is complicated by the time constant of the water flow control based on inside air temperature, which is less than 30 minutes [55], and the lag time of the heating system due to water transport in the pipes, which is in the order of 10 minutes [54]. With the 1-h time step,

this dynamics can be neglected and the radiator heating system can be modeled as direct heat input to the inside air, an approach that has passed validation by building experts and comparison with TRNSYS simulations [56].

- The computation time of the dynamic programming (DP) algorithm with the shiftable appliance model scales asymptotically as $O\left(\left(\frac{n_{h,shiftable}}{\Delta t}\right)^{n_{shiftable}+1}\right)$, hence the computational burden becomes high with a short time step and many shiftable appliances. Excluding shiftable appliances, the computation time scales linearly with the number of time steps, so the computation time is not as large an issue in that case, provided the time step is long enough so that the model doesn't have to be complicated because of validity.
- Electricity spot market prices are hourly. The hourly energy balances correspond to billing with hourly net metering, which is in use in e.g. Denmark [57], and the required legislation is under preparation in Finland [58], where the case study in this paper is situated.
- The variable condensing operating mode of a heat pump is considerably simpler to model when the time step is long compared to the time that a heat pump takes to stabilize to steady state, which is several minutes [59].
- The time scale of hours is relevant in the study of thermal dynamics of buildings.
- Hourly input data is often available. For example in the case study in this paper, the coarsest input data resolution is hourly. This is the case for representative domestic hot water (DHW) consumption data.

Because of the hourly time step, all the control variable values obtained from the model are hourly averages. Hence, the energy storage response to sub-hourly solar radiation variations is not directly considered. As the employed battery model is linear, the battery could partially smooth the sub-hourly variations without any effect on the model results. However, this is not the case for the TES and GSHP, which form a non-linear system as the COP of the GSHP depends on the TES temperature. In practice, both these storages could be used for smoothing of abrupt PV production variations with lower-level controllers which are not considered in this paper.

2.1. Heating system model

The modeled heating system (Fig. 2) consists of a GSHP with an auxiliary electric heater, a water tank as TES, and a hydronic system for space heating. This kind of system is typical in residential houses in Nordic countries and is also used in other kinds of buildings. In addition, DHW is heated with a heat exchanger in the TES and an auxiliary electric water heater in the fixed condensing mode,

or with the GSHP and a heat exchanger in a DHW storage in variable condensing mode. In variable condensing, GSHP heating is alternated between space heating and DHW heating with the three-way valve in Fig. 2 to optimize the coefficient of performance (COP) of the heat pump; in fixed condensing, the GSHP is connected directly to the TES. In the reference system with no TES, the GSHP is connected directly to the hydronic system and DHW is heated without preheating in the DHW storage.

The numerical model is based on calculating the mass and energy balances in the subsystems. Temperatures are modeled explicitly. The TES is modeled as fully mixed to enable reasonable computation time with the Dynamic Programming (DP) algorithm used for solving cost-optimal control. A detailed description of the model is given in Supplementary Information.

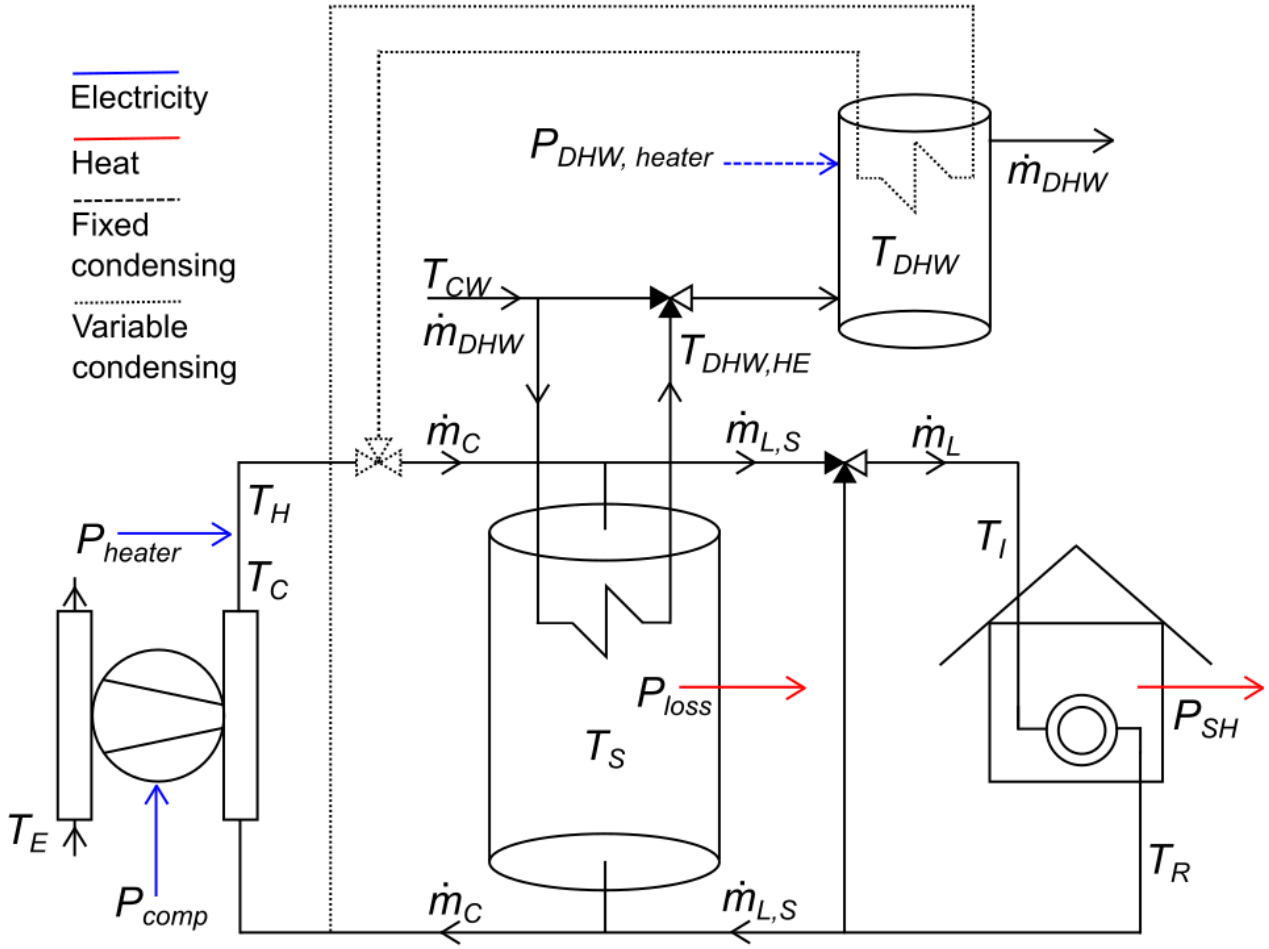

Figure 2. Model of the heating system ($\dot{m}$ = mass flows, T = temperatures, P = power flows). For details, see Supplementary Information. Symbols are in accordance with [60,61].

2.2. Electrical system model

An electrical topology in which all the loads, the battery and PV are connected to the same AC bus is employed (Fig. 3). This AC coupling is one of the two main layouts for battery connection with PV, the other being DC coupling with a common inverter for PV and the battery [43]. The battery is connected with a bidirectional inverter to allow for arbitrage in cost-optimal control in addition to storage of PV electricity. Single-phase powers are assumed small enough to comply with fuse current limits, and the electricity meter is assumed to perform net metering on all the three phases. The total three-phase power P_{net} is limited by the design grid connection capacity P_{max}.

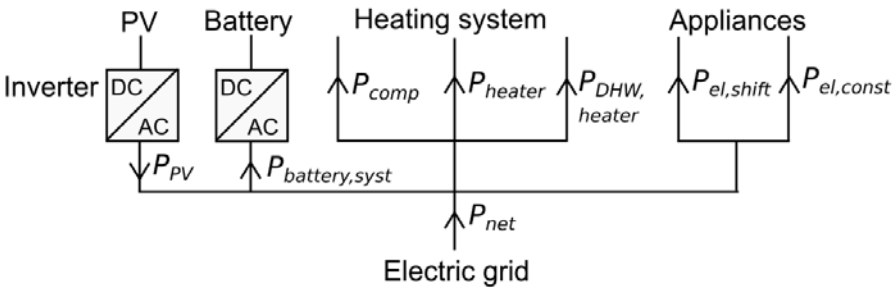

Figure 3. Electrical system layout.

The appliance electricity use is divided to a constant and a shiftable part (Fig. 3). Shiftable appliances (e.g. washing machines, dishwashers, tumblers) are modeled with an average demand cycle representing all the shiftable appliances in the building. The battery is modeled with a simple storage model. Detailed descriptions of the models are given in Supplementary Information.

3. System control algorithms for cost minimization and PV self-consumption maximization

The control of the flexible energy system is the key for capitalizing on the potential benefits from the different flexibility options available. Two control approaches are studied in this paper: cost-optimal control and rule-based control for PV self-consumption maximization. Fig. 4 shows a schematic of the control principles.

The purpose of cost-optimal control is to minimize total electricity cost to the building, and it represents an advanced control case in which the building takes the role of an active prosumer which both buys and sells electricity actively. The electricity cost is minimized over sequential 24-hour horizons, taking advantage of variations in PV production and hourly electricity market price. The additional constraint of zero grid infeed is also included as a separate case to study how a conventional unidirectional energy system, with the building acting as a conventional consumer, could be achieved with PV in flexible buildings and advanced control. In this case, any PV production that the flexible energy system of the building doesn't consume is curtailed. It has to be noted that the grid infeed limit is imposed on the energy balance over the 1-h time step in this study, and instantaneous infeed might occur even if the balance is zero.

The rule-based control maximizes PV self-consumption each hour by storing any surplus PV production to the electric and thermal storages and shiftable appliance runs. That is, the building attempts to avoid selling PV electricity and sells only when self-consumption fails due to limited flexibility of the energy system. As the price paid for sold electricity is lower than the cost of bought electricity in many markets, rule-based maximization of PV self-consumption can be expected to decrease the total electricity cost. Rule-based control is studied with two control modes: with and without an auxiliary electric resistance heater in the heat pump. The resistance heater allows for increased self-consumption, but lowers energy efficiency as it replaces heat production with the GSHP. Achieving a unidirectional energy system with the rule-based control is studied by dimensioning the storages sufficiently to allow for zero grid infeed.

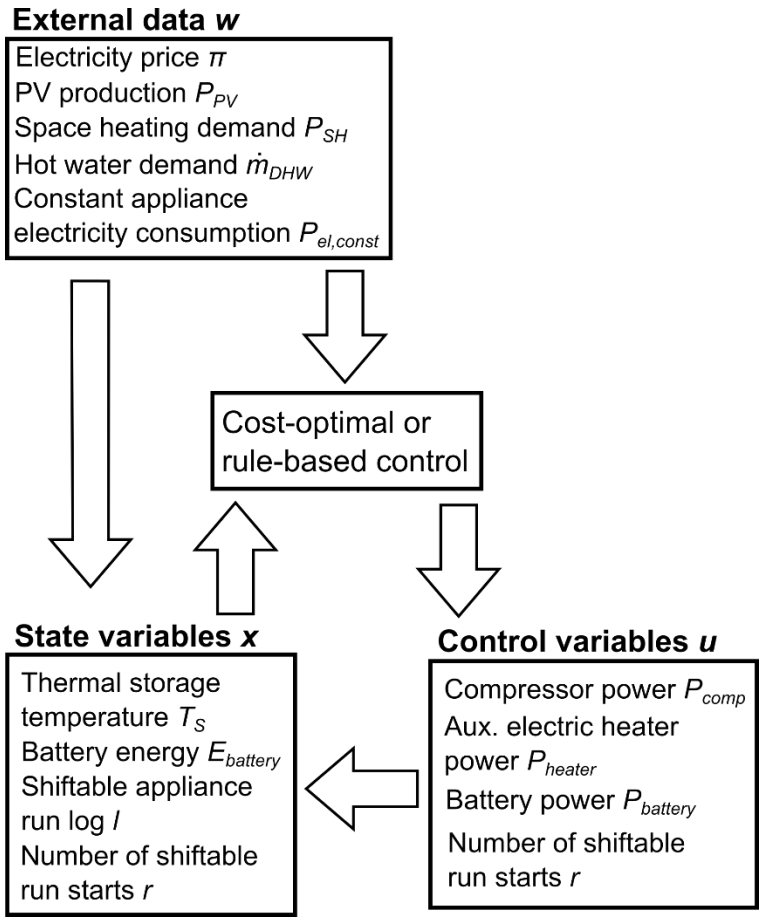

Figure 4. Schematic of the control principles for the building energy system. The cost-optimal control minimizes electricity cost over a 24-h time horizon and the rule-based control maximizes PV self-consumption on each time step.

3.1 Cost-optimal control

The cost-optimal control minimizes the total electricity cost in a 24-h horizon. In the full-year simulations, it is solved in sequential daily horizons from midnight to midnight. The arising optimal control problem is relatively challenging: The system equation of the thermal storage is nonlinear due to the temperature dependency of the COP of the heat pump, and the optimal control problem contains integer states and controls when shiftable loads are included. Moreover, the non-linear programming problem obtained by integrating the system equations is nonconvex. Hence, approximate global cost-optimal control u^* is solved with the deterministic Dynamic Programming (DP) algorithm [62] as a minimization problem of the objective function J which denotes total cost over the time horizon:

$$J_N(x_N) = g_N(x_N),\ x_N \in X_N \tag{1}$$

$$J_k(x_k) = \min_{u_k \in U_k(x_k)} [g_k(x_k, u_k, w_k) + J_{k+1}(x_{k+1})\,],$$
$$u_k^*(x_k) = \arg\min_{u_k \in U_k(x_k)} [g_k(x_k, u_k, w_k) + J_{k+1}(x_{k+1})\,], \quad (2)$$
$$k = 0,1,\dots,N-1,\ x_k \in X_k,$$

$$x_{k+1} = f_k(x_k, u_k, w_k). \quad (3)$$

The energy system state vector $x_k = \left[T_{S,k}, r_{k-(n_{h,shiftable}-1)}, \dots, r_{k-1}, l_k, E_{battery,k}\right]^T$ and the control vector $u_k = \left[P_{comp,k}, P_{heater,k}, P_{battery,k}, \dot{m}_{C,k}, r_k\right]^T$. The vector $w_k = \left[\pi_k, P_{PV,k}, P_{SH,k}, \dot{m}_{DHW,k}, P_{el,const,k}\right]^T$ contains external data, which is deterministic in this work as weather and consumption forecasts are assumed ideal. That is, exact information of the future weather and consumption data is assumed to be available prior to the optimization horizon. The obtained results represent the best possible case. The feasible sets of states X_k and controls $U_k(x_k)$ are defined by the constraints in Table 1, where $T_{S,min,k}$ is the input temperature of the hydronic system, or the cold water temperature when there is no space heating demand. As the feasible compressor power interval is continuous, an inverter-controlled heat pump is modeled here; in fixed condensing, the heat pump can be modeled without inverter control by allowing only on-off control of compressor power. Fig. 5 shows a flowchart description of the algorithm.

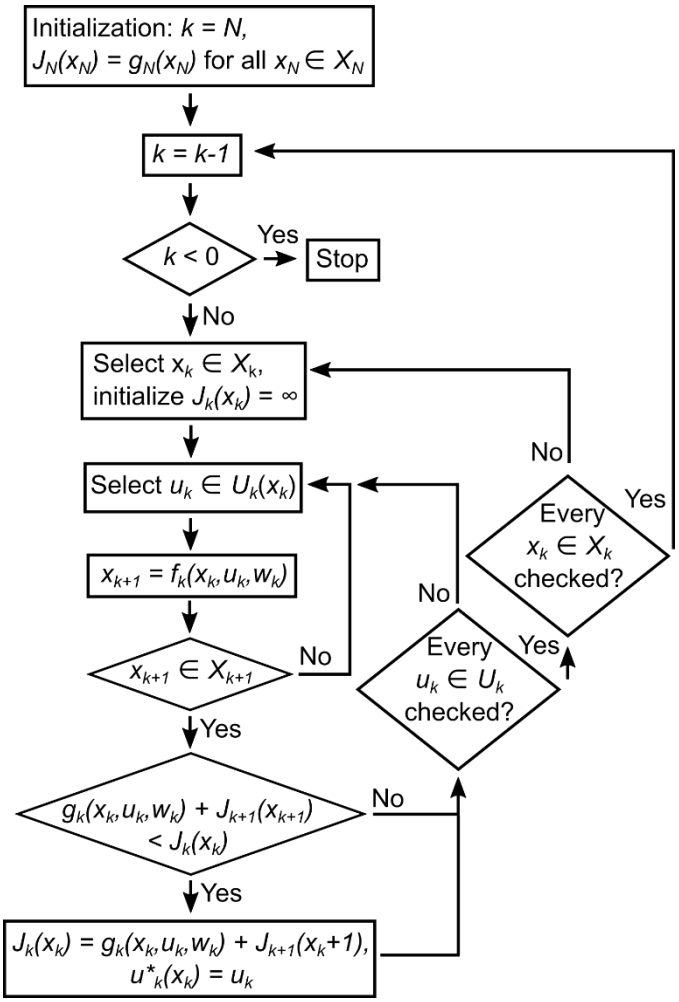

Figure 5. A flowchart of the DP algorithm.

J_k is the total cost function from the end of the horizon to the time step k. The cost incurred on time step k is

$$g_k(x_k, u_k, w_k) = \begin{cases} \pi_{prod,k} P_{net,k}, P_{net,k} \leq 0 \\ \pi_{cons,k} P_{net,k}, \text{otherwise,} \end{cases} \quad (4)$$

where the net power balance of the building with the grid is

$$P_{net,k} = P_{cons,k} - P_{PV,curtailed,k}, \quad (5)$$

$$P_{cons,k} = P_{comp,k} + P_{heater,k} + P_{DHW,heater,k} + P_{battery,syst,k} + P_{el,const,k} + \sum_{i=1}^{n_{h,shiftable}} r_{k-(n_{h,shiftable}-i)} P_{el,shift,i}. \quad (6)$$

The end cost is zero for all feasible end states, as no end state incurs any cost outside the optimization horizon:

$$g_N(x_N) = 0, \forall x_N \in X_N. \tag{7}$$

The state equation $x_{k+1} = f_k(x_k, u_k, w_k)$ contains the discretized state equation of the fully mixed TES model and the discrete state equations of the shiftable appliances and battery (see models in Supplementary Information). An hourly time step is used, with a sub-hourly integration time step for the TES model (see Supplementary Information for details).

Table 1. Constraints for the optimal control problem. See Supplementary Information for explanation of numerical values.

Physical temperature limits		
Storage	$T_{S,k} \in [T_{S,min,k}, 95\ °C], \forall k$	(8)
Heat pump condenser	$T_C \in [0,95]$ °C	(9)
Heat pump condenser	$T_C \in [0,65]$ °C if $P_{comp} > 0$	(10)
Heat pump output after auxiliary electric heater	$T_H \in [0,95]$ °C	(11)
Maximum mass flow through the heat pump condenser	$\dot{m}_C \in [0, 0.5\ ]$ kg/s.	(12)
Battery, heat pump compressor and auxiliary heater dimensioning		
Battery capacity	$E_{battery} \in [0, E_{battery,max}]$	(13)
Battery power	$P_{battery} \in [-E_{battery,max}, E_{battery,max}]$	(14)
Heat pump compressor power	$P_{comp} \in [0, P_{comp,max}]$	(15)
Heat pump auxiliary heater power	$P_{heater} \in [0, P_{heater,max}]$	(16)
No heating is allowed if there is no mass flow to transfer heat	$P_{comp} = 0$ and $P_{heater} = 0$ if $\dot{m}_C = 0$	(17)
Design grid connection capacity	$P_{net} \in [-P_{max}, P_{max}]$	(18)
PV production after curtailment		
If no grid feed-in allowed	$P_{PV,curtailed} = \min(P_{PV}, P_{cons})$	(19)
Otherwise	$P_{PV,curtailed} = P_{PV}$	(20)
Shiftable appliances		
Integer number of shiftable appliances up to the number available in the building can be started on each time step	$r_{k-(n_{h,shiftable}-i)} \in \{0,1,..,n_{shiftable}\},\ i = 1,..n_{h,shiftable}$	(21)
Not more simultaneously running appliances than available in the building	$\sum_{i=1}^{n_{h,shiftable}} r_{k-(n_{h,shiftable}-i)} \leq n_{shiftable}$	(22)
Appliances cannot be started so that they would run outside the optimization horizon	$r_k = 0,\ k = N - i, i = 1,..n_{h,shiftable} - 1$	(23)
Appliance run log takes integer values and cannot exceed total number of runs in the optimization horizon	$l_k \in \{0,1, \dots, n_{runs,shiftable,k} - 1, n_{runs,shiftable,k}\}, \forall k$	(24)
Appliance run log is zero in the beginning of the horizon	$l_k = 0, k = 0$	(25)
All appliance runs in the horizon have to be performed	$l_k = n_{runs,shiftable,k}, k = N$	(26)

The continuous states and controls are discretized with the following step sizes in the case study in this paper: $\Delta E_{battery}$ = 0.5 kWh, $\Delta P_{battery} = \Delta P_{comp} = \Delta P_{heater}$ = 0.5 kW, ΔT_S = 2 °C, $\Delta \dot{m}_C$ = 0.125 kg/s. The power discretization steps are equal so that they are comparable options for PV balancing in the optimization. Only minor improvement in the total electricity cost was noticed in tests with finer power and battery energy discretization. Discretized state and control vectors related to the flexibility sources left out of the studied configuration are replaced by zero-valued singletons (except $T_{S,min,k}$-valued singleton in case of T_S). The arising look-up tables are interpolated bilinearly in the continuous states T_S and $E_{battery}$.

The computation time is highly dependent on the included flexibility sources (TES, battery, appliance shifts), as the computation time of the DP algorithm scales in the product of discrete states in each dimension. With the dimensions of the case study in this paper and TES as the only flexibility source, annual optimal control in sequential 24-h horizons is solved in 30 seconds with a parallel implementation in C with a four-core Intel Xeon E3-1230 V2 3.3 GHz processor. Including more flexibility sources rapidly increases the computation time and high-performance computing is required in the high end.

3.2 Rule-based control

The simple rule-based control aims at maximizing the PV self-consumption directly and via battery and thermal storage. The same constraints as in the optimal control problem are satisfied as they are physical constraints of the studied system, with the exception of (23), which is due to the finite horizon in the cost-optimal control.

With a fixed condensing heat pump, the reference control for heating the TES with the heat pump keeps the TES temperature at a given constant setpoint. This control requires no forecasts. With variable condensing, the setpoint is $T_{S,min,k}$, obtained from the input temperature of the hydronic system. That is, ideal 1-h ahead forecasts of the outdoor temperature and space heating demand are assumed available in this case. Shiftable loads are run according to the original schedule and the battery is unused in the reference control. The mass flow through the heat pump condenser follows on/off control between zero and the maximum value depending on heating power.

If there is surplus PV power available after the reference control at each time step, the energy is self-consumed in the following priority:

1. Shiftable appliances in the shifting time window (24 h, between midnights) are moved to consume the surplus;
2. The remaining surplus is stored in the battery;
3. The remaining surplus is converted to heat and stored in the TES by increasing P_{comp} by the surplus;
4. If the auxiliary electric heater of the heat pump is used in the control in addition to the heat pump, the remaining surplus is converted to heat and stored in the TES by increasing P_{heater} by the surplus.

At times when the PV power does not cover all consumption, the battery is discharged and only the deficit is drawn from the grid.

4. Case study and input data

The simulations made to test the model are based on measured total and appliance-level electricity consumption and building properties of a real residential low-energy detached house located in Porvoo, Finland (60.4° N, 25.7° E) [63]. The simulations are run over a full year from January 2013 to January 2014.

4.1 External data

Meteorological data comprising direct and diffuse solar radiation on a horizontal plane, temperature and 10-minute-average wind speed was obtained from the Finnish Meteorological Institute [64]. Data from the Kumpula weather station (60.20° N, 24.96° E) was used, with missing values in temperature and wind speed filled with data from the close-by Kaisaniemi station (60.18° N, 24.94° E). Missing values in the solar radiation data were interpolated linearly.

Two types of pricing schemes are used in this paper: real-time pricing following the stock market price of electricity for optimal control and constant pricing for rule-based and reference controls. Hourly electricity stock market prices for Finland in the day-ahead market Elspot [65] are used with a utility margin [66], averaging 5.4 c/kWh in total. For the constant energy price, a representative value of 6.7 c/kWh is used, obtained as the average price of permanent contract offers for a detached house in Finland in 2013 [67]. In addition to the energy price, the consumer has to pay distribution cost [68] and excise tax and supply security charge [69], totaling 5.1 c/kWh in 2013 and 5.3 c/kWh in 2014. Value added tax is included in the consumption costs. The price paid by Finnish utilities for residential electricity production fed to the distribution grid is the hourly stock market price subtracted

by utility commission [70]. The prosumer has to pay the distribution cost of production [71]. The average net value in this case is 3.8 c/kWh.

4.2 Building and heating system properties and energy consumption

The space heating load P_{SH} of the building and the electricity production of a 1-kW_p PV system were simulated with ALLSOL [72,73] in 1-hour time steps with hourly averages of the meteorological data. The PV system produces 873 kWh/kW_p annually. The inclination of the PV array was 30° and the azimuth due south. *U* values and dimensions were obtained from energy inspection results, and measured electricity consumption was used for appliance heat generation.

An annual time series of DHW use was constructed from a representative average daily DHW consumption in a Finnish single-family house [74], scaled to total annual consumption in the house (6833 kWh) [63]. Country-specific data is necessary here as the daily consumption profile in Finland is markedly different from other countries [75].

Hourly total electricity consumption over the full year (annual total 7918 kWh), and the 8–9-day appliance-level consumption time series of three of the four available shiftable appliances, namely washing machine, tumbler and one of the two dishwashers in the house were measured on-site [76]. The appliance demand cycles lasted 3 hours at maximum, so the data was averaged to a 3-hour demand cycle to avoid overlaps in the optimized appliance schedules. Runs of the shiftable appliances were identified in the annual total consumption data with the algorithm described in Supplementary Information.

The design grid connection capacity is assumed P_{max} = 24.15 kW, from three-phase power with typical 35 A fuses. The GSHP compressor power is dimensioned at 2.5 kW in the model to fully cover the space heating and domestic hot water load with the medium-temperature heating system. The auxiliary electric heater of the GSHP is dimensioned at 10 kW.

5. Results

Flexibility of the residential energy system to integrate PV is studied with two PV system sizes in the size range of typical commercial systems [77]. 3 kW_p is three times the hourly self-use limit and allows for considerable increase in PV production from the self-use limit with complete self-consumption with small-size storage. 9 kW_p covers the whole annual appliance electricity consumption of the building.

Fixed condensing heat pump operation with a medium-temperature heating system is studied with both PV sizes. Even though variable condensing is more energy efficient, fixed condensing installations are also used [78], and always include storage for space heating and domestic hot water that can be used for flexibility. The medium-temperature heating system (max. 60 °C) matches the DHW temperature in fixed condensing, and requires less radiator area than a lower temperature system. The effect of a low-temperature heating system and variable condensing are also studied with the 9-kW_p PV system. The lower temperature in the heating system allows for more flexibility with the TES, and variable condensing is more energy-efficient than fixed condensing. Fig. 6 shows the cases in graphical form. The 0.3 m^3 TES used in the reference cases for fixed condensing heat pump connection is a typical size for a small commercial thermal storage [79].

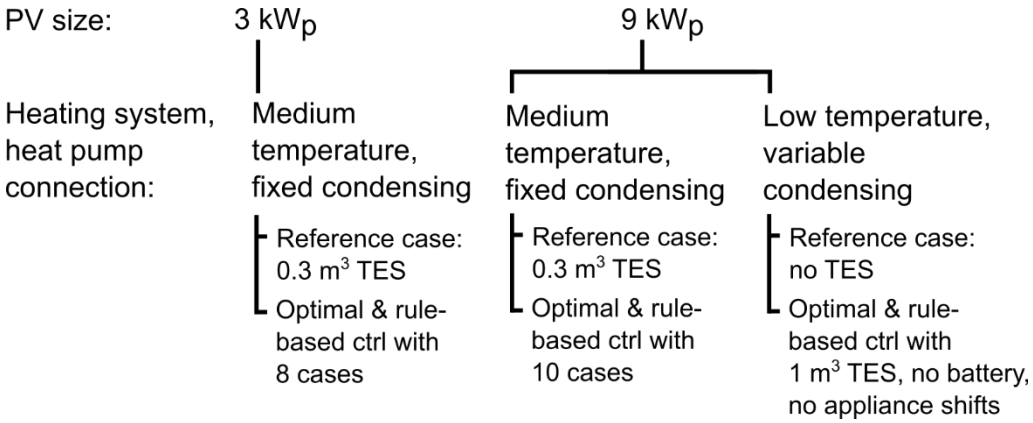

Figure 6. Cases studied in this paper.

Three parameters are used to judge the annual operation of the system: total electricity cost, total grid feed-in, and total annual electricity balance. The last metric is the total PV production after possible curtailment subtracted by the total annual consumption, and it indicates the effects that the controls have on energy consumption and PV curtailment.

5.1. Case: 3-kW_p PV system

With the 3-kW_p PV system, the reference case is a 0.3 m^3 TES used for DHW production with the heat pump. The reference control is simple and inflexible: the TES temperature is kept at 60 °C setpoint, and no battery or appliance shifts are used. This configuration can cover the space heating and DHW consumption with the heat pump. The 3-kW_p system produces annually 2620 kWh, which corresponds to 33% of the total appliance electricity consumption or 19% of the total electricity consumption including heating in the reference case. 20% of the PV production need to be fed to the grid due to production and consumption mismatch.

The annual electricity cost, grid feed-in and electricity balance relative to the reference case are presented in Fig. 7. The four storage dimensions are selected to show the effect of an increase in TES size from the reference configuration and adding substantial short-term battery storage. The heat pump and resistance heater can bring grid feed-in to zero with this PV system size already with a 0.3 m^3 TES. Increasing the TES size and including a 1 kWh/kW_p battery decreases considerably the grid feed-in if the auxiliary resistance heater is not used.

The cost-optimal control provides a 13–15% decrease in the yearly electricity cost, along with a 36–88% decrease in the grid feed-in compared to the reference case. If no electricity is allowed to be fed into the grid, the cost-optimal control can provide almost equal cost savings. The battery and increasing the TES size affect the electricity cost very little in this case. While adding appliance shifts can decrease grid feed-in by 11% at maximum in these cases, its effect on the electricity cost is minor.

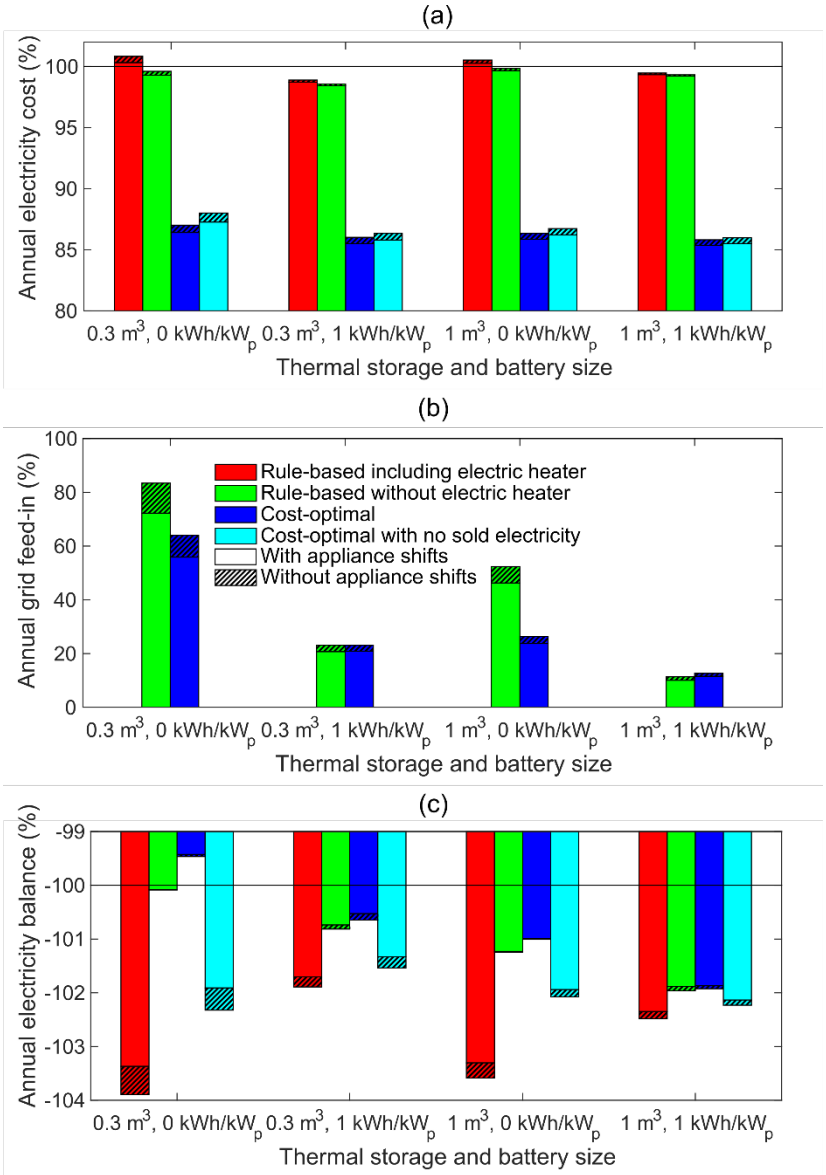

Figure 7. Simulation results with a 3-kW_p PV system: (a) Annual electricity cost relative to the reference case (1344 €), (b) grid feed-in relative to the reference case (537 kWh) and (c) electricity balance relative to the reference case (-11039 kWh). The heating system is medium-temperature and the heat pump is connected in fixed condensing.

5.2 Case: 9-kW_p PV system

Two heating system temperature levels (max. 60 °C and max. 40 °C, see full control curves in Supplementary Information) are studied with the 9-kW_p PV system, the former with a heat pump connected in fixed condensing and the latter with variable condensing. The medium-temperature heating system (max. 60 °C) matches the DHW temperature in fixed condensing. The lower temperature in the max. 40 °C heating system allows for more flexibility with the TES, and variable condensing is more energy-efficient than fixed condensing.

5.2.1 Medium-temperature heating system with fixed condensing

The reference case is the same as in the 3-kW_p case: a 0.3 m^3 TES used for DHW production with the heat pump, with TES temperature kept at 60 °C setpoint in the reference control, no battery, and no appliance shifts. The 9-kW_p PV system produces annually 7860 kWh, corresponding to 99% of the total appliance electricity consumption or 58% of the total electricity consumption including heating in the reference case, with 60% of the PV electricity fed to the grid.

Fig. 8 shows the annual cost, grid feed-in and annual total electricity balance relative to the reference case for several system configurations with 9 kW_p PV. The system parameters have been selected to represent the range of storage sizes from the base case configuration to storages required to bring grid feed-in to zero without curtailment; they are not intended for systematic comparison between storage sizes.

The cost-optimal control provides a 17–25% cost reduction, along with 8–52% decrease in grid feed-in. When constrained to zero grid feed-in, cost savings drop to 2–15%, and the decrease in annual electricity balance is substantial due to PV curtailment, storage losses and GHSP heating being replaced by resistance heating.

The rule-based control including the auxiliary electric resistance heater in the heat pump can effectively self-consume the PV production, with increased cost compared to the reference case if a

battery is not used, and a substantial decrease in the annual electricity balance due to storage losses and heat pump heating being replaced by the resistor. The decrease in grid feed-in achieved with the rule-based control without the resistance heater is approximately the same as with cost-optimal control.

Increasing the TES size decreases the optimal electricity cost in small storage sizes, but with the 2.5 m^3 TES the cost increases due to increased losses. Increasing the battery size decreases the electricity cost. Grid feed-in decreases with increasing storage size. The effect of the appliance shifts is minor.

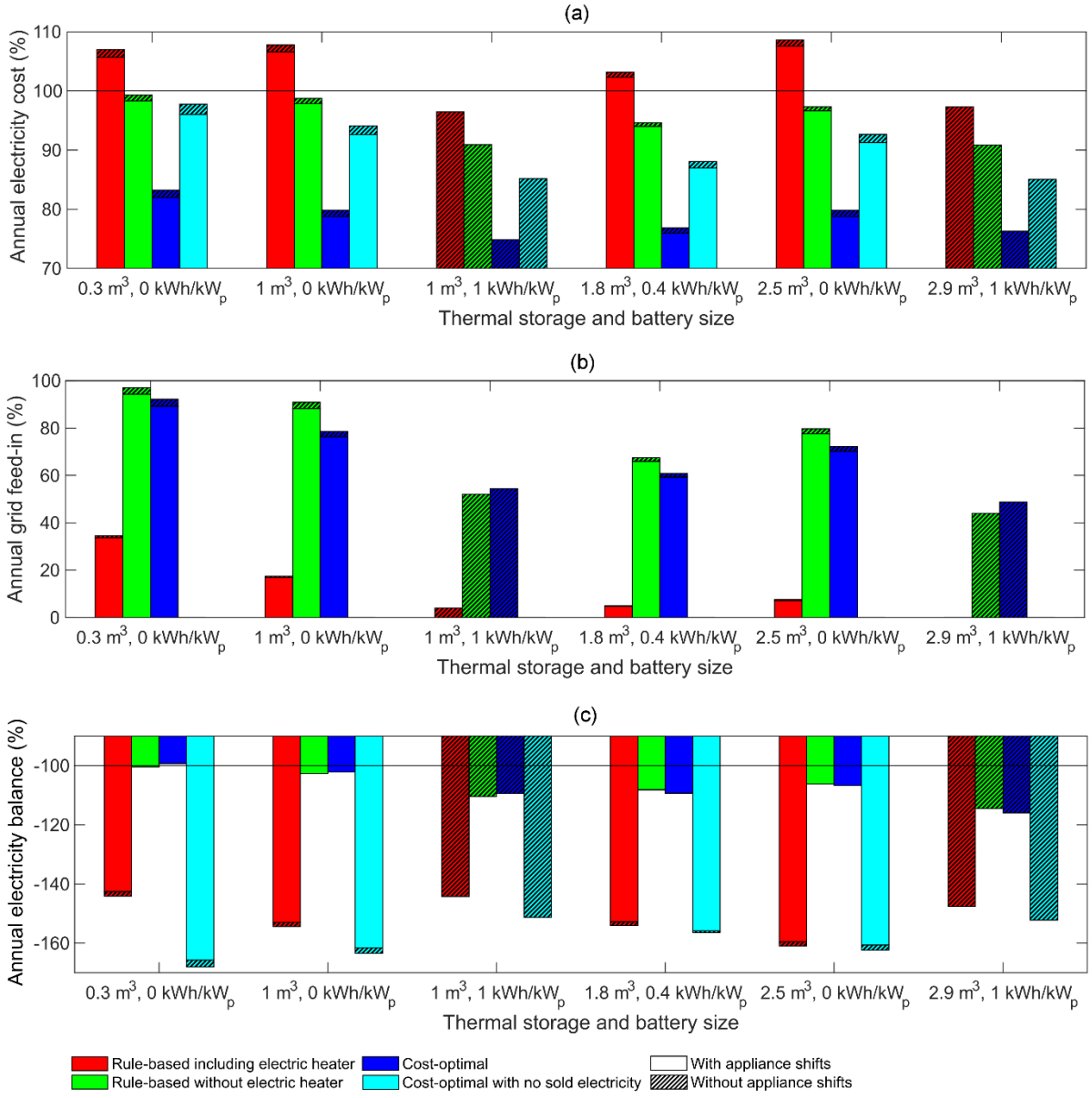

Figure 8. Simulation results with a 9-kW_p PV system: (a) Annual electricity cost relative to the reference case (1041 €), (b) grid feed-in relative to the reference case (4763 kWh) and (c) electricity

balance relative to the reference case (-5799 kWh). The heating system is medium-temperature and the heat pump is connected in fixed condensing.

The effect of cost-optimal control on the power duration of the dwelling is demonstrated in Fig. 9. The cost-optimal control shifts draws and feed-in of electricity towards peak hours as it takes advantage of price changes. With a battery, the shift is more dramatic and peak import and export powers are increased as well. As shown in Fig. 10, the peak power draws occur during low-price hours and peak feed-in during high-price hours, hence the control contributes to balancing energy system operation despite increases in peak power magnitudes.

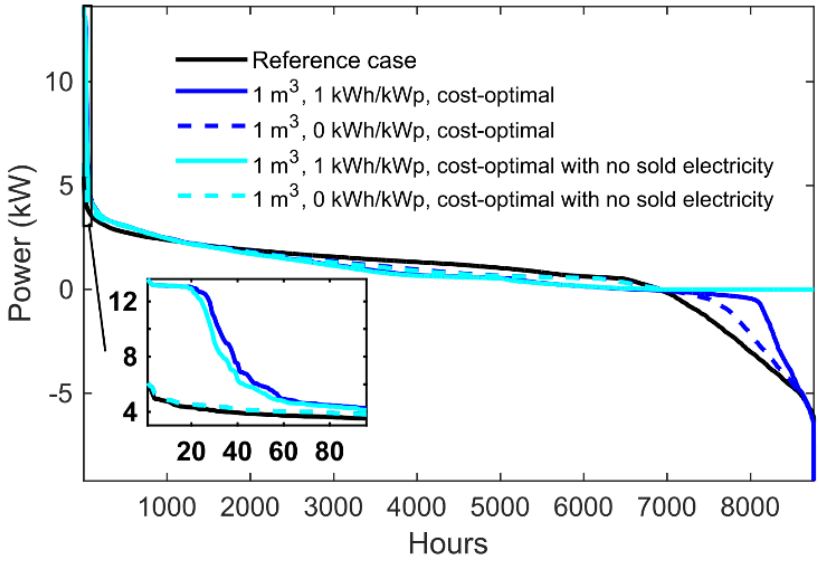

Figure 9. Power duration curve with a 9-kW_p PV system, a medium-temperature heating system and a fixed-condensing heat pump. Positive power is drawn from the grid and negative fed to the grid.

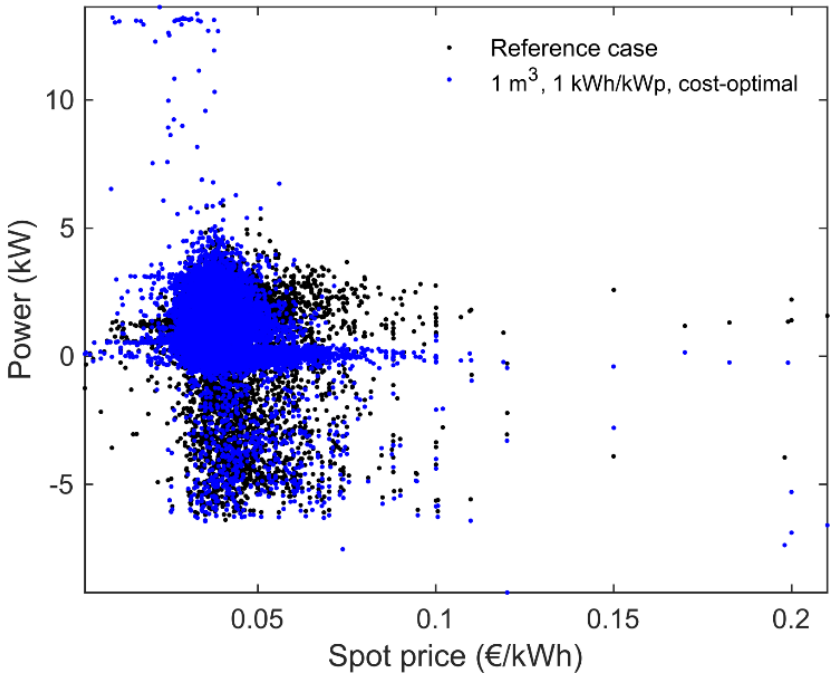

Figure 10. Scatter plot of the hourly power balance with a 9-kW_p PV system, a medium-temperature heating system and a fixed-condensing heat pump. Positive power is drawn from the grid and negative fed to the grid.

5.2.2. Low-temperature heating system with variable condensing

The reference case of a variable condensing system has no TES, as it is not needed for DHW provision. Moreover, there is no battery and no appliance shifts are used. 7860 kWh, corresponding to 64% of the total electricity consumption is provided with a 9-kW_p PV system in the reference case, and 62% of the PV production is fed to the grid. A 1 m^3 TES is added to the system for flexibility provision, dimensioned for comparison with the results for a medium-temperature heating system.

Variable condensing with a low-temperature system provides 14% reduction in annual electricity cost and 22 % increase in annual electricity balance in the reference case compared to fixed condensing and a medium-temperature system, demonstrating the increase in energy efficiency.

With the TES for flexibility, optimal control provides a 19% cost decrease and decreases grid feed-in by 16% compared to the reference case (Figure 11). Constrained to zero grid feed-in, the cost decrease drops to 3%, with a substantial decrease in annual electricity balance due to increased curtailment and electricity consumption.

Compared to fixed condensing with a medium-temperature heating system, the annual costs in the control cases are 11-20% lower and annual electricity balances 11-22% higher. The effect of increased flexibility with the heat pump and TES is especially visible in rule-based control without the resistance heater, which achieves 17% lower grid feed-in. Cost-optimal control feeds 9% more electricity to the grid, however.

All DHW heating can be done with the GSHP in the variable condensing mode, therefore the DHW consumption affects the cost-optimal control less than in the fixed condensing mode. This is demonstrated through the correlation between the absolute TES temperature and the DHW mass flow, which is 0.32 in fixed condensing with a medium-temperature heating system, and 0.20 in variable condensing.

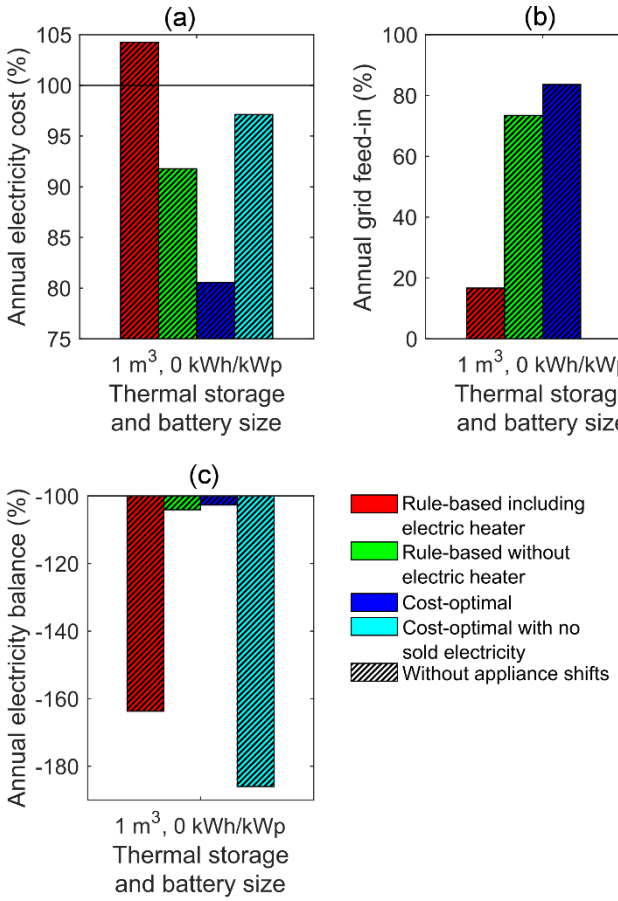

Figure 11. Simulation results with a 9-kW_p PV system: (a) Annual electricity cost relative to the reference case (896 €), (b) grid feed-in relative to the reference case (4869 kWh), and (c) electricity balance relative to the reference case (-4512 kWh). The heating system is low-temperature and the heat pump is connected in variable condensing.

6. Conclusions

A physically realistic model has been presented for cost-optimal and self-consumption maximizing rule-based control analysis of a flexible residential energy system with photovoltaics. The flexibility sources in the system are a ground-source heat pump with an auxiliary electric resistance heater and thermal energy storage, a battery and shiftable appliances.

The model is generic and applicable for an arbitrary condition. A case study of a Finnish low-energy house was conducted to demonstrate the use of the model and to investigate the effects of the controls. Significant electricity cost savings of 13–25%, along with 8–88% decrease in electricity fed to the grid with cost-optimal control were found, depending on PV capacity and the chosen flexibility sources. For 3 kW_p PV, the studied storage capacities were 0.3 and 1 m^3 TES, and 0 and 1 kWh/kW_p battery. For 9 kW_p PV, the storage capacities were in the ranges 0.3-2.9 m^3 and 0-1 kWh/kW_p. Most of the storage combinations were studied with and without appliance shifts.

Grid feed-in could also be effectively limited to zero at hourly level with cost-optimal or rule-based control, at the expense of smaller savings or even an increase in electricity cost, and less energy-efficient control due to increased electricity use and PV curtailment. The decrease in energy efficiency was minor with a 3-kW_p PV system (3x self-use limit), but substantial with a 9-kW_p PV system that could cover the total annual appliance electricity use of the building.

The heat pump with thermal storage and a battery were found more effective to provide flexibility than the shiftable appliances in the case study with a residential building. As their potential was found significant, further work will be done to study more thoroughly the effect of their dimensioning on the achieved cost savings and grid interaction. Moreover, further model and controller development including the effect of forecast error could be motivated. Heuristics responsive to price and PV production could be fruitful in achieving part of these benefits will less computational complexity than mathematical optimization.

The requirements of the power grid and energy system could be included explicitly in further work. Adequate but not excessive feed-in limitations based on system requirements would be beneficial as limiting grid feed-in to zero was noticed to give rise to considerably less energy-efficient control with a substantial PV installation. Even though cost-optimal control increases peak powers, peak feed-in

occurs during high-price periods and peak draws during low-price periods, hence the effect to the operation of the whole energy system is stabilizing in principle.

Acknowledgements

Mr. Kristian Bäckström from Posintra Oy and Mr. Olli Jalonen from Aalto University, Department of Industrial Engineering and Management are gratefully acknowledged for providing data for the case study, and Dr. Imran Asghar, Mr. Juuso Lindgren and Mr. Sakari Lepikko from Aalto University, Department of Applied Physics for providing measurement data on Li-ion battery operation for verification of the battery model in this work. Computational resources provided by Aalto Science-IT project are acknowledged. This research was funded by the Academy of Finland within the project CONICYT (13269795) and Aalto University Energy Science Initiative (ESCI) within the project GREEN ICT (9023621).

References

[1] IEA PVPS. Snapshot of Global PV Markets 2014. 2015.

[2] SolarPower Europe. Global Market Outlook for Solar Power 2015-2019. 2015.

[3] European Photovoltaic Industry Association. Global Market Outlook for Photovoltaics 2014-2018. 2014.

[4] Chandler H. Harnessing Variable Renewables: A Guide to the Balancing Challenge. Paris, France: IEA; 2011.

[5] Bessa R, Moreira C, Silva B, Matos M. Handling renewable energy variability and uncertainty in power systems operation. Wiley Interdiscip Rev Energy Environ 2014;3:156–78.

[6] Tuohy A, Kaun B, Entriken R. Storage and demand-side options for integrating wind power. Wiley Interdiscip Rev Energy Environ 2014;3:93–109.

[7] Holttinen H. Wind integration: experience, issues, and challenges. Wiley Interdiscip Rev Energy Environ 2012;1:243–55.

[8] Riesz J, Milligan M. Designing electricity markets for a high penetration of variable renewables. Wiley Interdiscip Rev Energy Environ 2015;4:279–89.

[9] Lund PD, Lindgren J, Mikkola J, Salpakari J. Review of energy system flexibility measures to enable high levels of variable renewable electricity. Renew Sustain Energy Rev 2015;45:785–807.

[10] Kubik ML, Coker PJ, Barlow JF. Increasing thermal plant flexibility in a high renewables power system. Appl Energy 2015;154:102–11. doi:10.1016/j.apenergy.2015.04.063.

[11] Moura PS, de Almeida AT. The role of demand-side management in the grid integration of wind power. Appl Energy 2010;87:2581–8. doi:10.1016/j.apenergy.2010.03.019.

[12] Nistor S, Wu J, Sooriyabandara M, Ekanayake J. Capability of smart appliances to provide reserve services. Appl Energy 2014. doi:10.1016/j.apenergy.2014.09.011.

[13] Drysdale B, Wu J, Jenkins N. Flexible demand in the GB domestic electricity sector in 2030. Appl Energy 2014;139:281–90. doi:10.1016/j.apenergy.2014.11.013.

[14] Schroeder A. Modeling storage and demand management in power distribution grids. Appl Energy 2011;88:4700–12. doi:10.1016/j.apenergy.2011.06.008.

[15] Niemi R, Mikkola J, Lund PD. Urban energy systems with smart multi-carrier energy networks and renewable energy generation. Renew Energy 2012;48:524–36.

[16] Lund PD, Mikkola J, Ypyä J. Smart energy system design for large clean power schemes in urban areas. J Clean Prod 2015;103:437–45.

[17] Lund PD. Clean energy systems as mainstream energy options. Int J Energy Res 2015. doi:10.1002/er.3283.

[18] Lund P. Large-scale urban renewable electricity schemes – Integration and interfacing aspects. Energy Convers Manag 2012;63:162–72.

[19] Lund PD, Mikkola J. Increasing the share of PV by a factor of 2-3 over the self-use limit through urban electricity-to-thermal conversion schemes. In: Betancourt U, Ackermann T, editors. Proc. 3rd Int. Work. Integr. Sol. Power into Power Syst., London: Energynautics GmbH; 2013.

[20] Mikkola J, Salpakari J, Ypyä J, Lund P. Increasing the Solar Share through Smart Matching of PV, Load and Energy Infrastructure in Urban Context. In: Betancourt U, Ackermann T, editors. Proc. 4th Int. Work. Integr. Sol. Power into Power Syst., Berlin: Energynautics GmbH; 2014.

[21] Hewitt NJ. Heat pumps and energy storage – The challenges of implementation. Appl Energy 2012;89:37–44. doi:10.1016/j.apenergy.2010.12.028.

[22] Waite M, Modi V. Potential for increased wind-generated electricity utilization using heat pumps in urban areas. Appl Energy 2014. doi:10.1016/j.apenergy.2014.04.059.

[23] Blarke MB. Towards an intermittency-friendly energy system: Comparing electric boilers and heat pumps in distributed cogeneration. Appl Energy 2012;91:349–65. doi:10.1016/j.apenergy.2011.09.038.

[24] IEA-PVPS. Trends in Photovoltaic Applications 2014. 2014.

[25] Stetz T, Marten F, Braun M. Improved low voltage grid-integration of photovoltaic systems in Germany. 2013 IEEE Power Energy Soc Gen Meet 2013;4:1–1.

[26] Bayer P, Saner D, Bolay S, Rybach L, Blum P. Greenhouse gas emission savings of ground source heat pump systems in Europe: A review. Renew Sustain Energy Rev 2012;16:1256–67.

[27] Arteconi A, Hewitt NJ, Polonara F. State of the art of thermal storage for demand-side management. Appl Energy 2012;93:371–89.

[28] Ferreira HL, Garde R, Fulli G, Kling W, Lopes JP. Characterisation of electrical energy storage technologies. Energy 2013;53:288–98.

[29] Nykvist B, Nilsson M. Rapidly falling costs of battery packs for electric vehicles. Nat Clim Chang 2015;5:100–3.

[30] Bruni G, Cordiner S, Mulone V, Rocco V, Spagnolo F. A study on the energy management in domestic micro-grids based on Model Predictive Control strategies. Energy Convers Manag 2015. doi:10.1016/j.enconman.2015.01.067.

[31] Wu Z, Xia X. Optimal switching renewable energy system for demand side management. Sol Energy 2015;114:278–88.

[32] Zhang Y, Hanby V. Model-based control of renewable energy systems in buildings. HVAC&R Res 2006;12:739–60.

[33] Zhao Y, Lu Y, Yan C, Wang S. MPC-Based Optimal Scheduling of Grid-Connected Low Energy Buildings with Thermal Energy Storages. Energy Build 2014. doi:10.1016/j.enbuild.2014.10.019.

[34] Anvari-Moghaddam A, Monsef H, Rahimi-Kian A. Cost-Effective and Comfort-Aware Residential Energy Management under Different Pricing Schemes and Weather Conditions. Energy Build 2014. doi:10.1016/j.enbuild.2014.10.017.

[35] Brahman F, Honarmand M, Jadid S. Optimal Electrical and Thermal Energy Management of a Residential Energy Hub, Integrating Demand response and Energy Storage System. Energy Build 2014;90:65–75.

[36] Barbato A, Capone A. Optimization Models and Methods for Demand-Side Management of Residential Users: A Survey. Energies 2014;7:5787–824.

[37] Cao S, Hasan A, Sirén K. Analysis and solution for renewable energy load matching for a single-family house. Energy Build 2013;65:398–411.

[38] Binder J, Williams CO, Kelm T. Increasing PV self-consumption, domestic energy autonomy and grid compatibility of PV systems using heat-pumps, thermal storage and battery storage. Proc. 27th Eur. Photovolt. Sol. Energy Conf. Exhib., Frankfurt, Germany: 2012, p. 4030–4.

[39] Vrettos E, Witzig A, Kurmann R, Koch S, Andersson G. Maximizing Local PV Utilization using small-scale batteries and flexible thermal loads. 28th Eur. Photovolt. Sol. energy Conf. Exhib., Paris, France: 2013, p. 4515–26.

[40] Verbruggen B, Driesen J. Grid Impact Indicators for Active Building Simulations. IEEE Trans Sustain Energy 2015;6:43–50.

[41] Widén J, Wäckelgård E, Lund PD. Options for improving the load matching capability of distributed photovoltaics: Methodology and application to high-latitude data. Sol Energy 2009;83:1953–66.

[42] Kootstra M a., Tong S, Park JW. Photovoltaic grid stabilization system using second life lithium battery. Int J Energy Res 2015. doi:10.1002/er.3310.

[43] Luthander R, Widén J, Nilsson D, Palm J. Photovoltaic self-consumption in buildings: A review. Appl Energy 2015;142:80–94.

[44] Wang C, Zhou Y, Jiao B, Wang Y, Liu W, Wang D. Robust optimization for load scheduling of a smart home with photovoltaic system. Energy Convers Manag 2015:1–11.

[45] Guo Y, Pan M, Fang Y. Optimal Power Management of Residential Customers in the Smart Grid. IEEE Trans Parallel Distrib Syst 2012;23:1593–606.

[46] Widén J, Munkhammar J. Evaluating the benefits of a solar home energy management system: impacts on photovoltaic power production value and grid interaction. Proc. eceee 2013 Summer Study, Presqu'île de Giens, France: 2013, p. 1223–33.

[47] Widén J. Improved photovoltaic self-consumption with appliance scheduling in 200 single-family buildings. Appl Energy 2014;126:199–212.

[48] Masa-Bote D, Castillo-Cagigal M, Matallanas E, Caamaño-Martín E, Gutiérrez A, Monasterio-Huelín F, et al. Improving photovoltaics grid integration through short time forecasting and self-consumption. Appl Energy 2014;125:103–13.

[49] Li J, Danzer M a. Optimal charge control strategies for stationary photovoltaic battery systems. J Power Sources 2014;258:365–73.

[50] Schreiber M, Hochloff P. Capacity-dependent tariffs and residential energy management for photovoltaic storage systems. 2013 IEEE Power Energy Soc. Gen. Meet., Vancouver, BC: IEEE; 2013, p. 1–5.

[51] Matthiss B, Müller D, Binder J, Pietruschka D. Model predictive control schemes for PV storage systems to increase grid compatibiltiy and optimize energy costs. EU PVSEC Proc., 2014, p. 3581–6.

[52] Salom J, Widén J, Candanedo J, Lindberg KB. Analysis of grid interaction indicators in net zero-energy buildings with sub-hourly collected data. Adv Build Energy Res 2015;9:89–106.

[53] Cao S, Sirén K. Impact of simulation time-resolution on the matching of PV production and household electric demand. Appl Energy 2014;128:192–208. doi:10.1016/j.apenergy.2014.04.075.

[54] Karlsson F, Fahlén P. Impact of design and thermal inertia on the energy saving potential of capacity controlled heat pump heating systems. Int J Refrig 2008;31:1094–103.

[55] Seppänen O. Building heating (in Finnish). 2nd ed. Helsinki: SuLVI ry; 2001.

[56] Oldewurtel F, Parisio A, Jones CN, Gyalistras D, Gwerder M, Stauch V, et al. Use of model predictive control and weather forecasts for energy efficient building climate control. Energy Build 2012;45:15–27. doi:10.1016/j.enbuild.2011.09.022.

[57] Kjær SB, Benz CH, Gonlazez A. Impact of New Danish Hourly Based Net Metering on the Acceptable Solar PV System Cost. 28th Eur. Photovolt. Sol. Energy Conf. Exhib., Paris, France: 2013, p. 4547–51.

[58] Ministry of Employment and the Economy. Renewal of statutes concerning accounting and metering of electricity deliveries (in Finnish). Legis Initiat 2015. https://www.tem.fi/ajankohtaista/vireilla/lainsaadantohankkeet/lainsaadantohankehaku?offset=1&xmid=5417 (accessed September 1, 2015).

[59] SENERA Oy. Ground heat (in Finnish) 2015. http://www.senera.fi/Maalampo/ (accessed May 25, 2015).

[60] Forsström J, Lund P. Optimization of operating strategies in a community solar heating system. Appl Math Model 1985;9:117–24.

[61] Ministry of the Environment. National Building Code of Finland. D4 HEPAC drawings (in Finnish). Finland: 1978.

[62] Bertsekas DP. Dynamic Programming and Optimal Control, Volume I. 3rd ed. Belmont, Massachusetts: Athena Scientific; 2005.

[63] Bäckström K. Smart building engineering. Sustainable housing and environment (K-EASY), final report (in Finnish). 2014.

[64] Finnish Meteorological Institute. The Finnish Meteorological Institute's open data 2014. https://en.ilmatieteenlaitos.fi/open-data (accessed May 30, 2014).

[65] Nord Pool Spot 2014. http://www.nordpoolspot.com/ (accessed April 9, 2014).

[66] Fortum. Fortum Tarkka - electricity price (in Finnish) 2014. http://www.fortum.com/countries/fi/yksityisasiakkaat/hinnastot/sahkosopimuksen-hinta-tarkka/pages/default.aspx (accessed July 1, 2014).

[67] Energy Authority. Electricity price statistics (in Finnish) 2015. http://www.energiavirasto.fi/sahkon-hintatilastot (accessed April 17, 2015).

[68] Porvoon Energia. Electricity contracts valid until further notice (in Finnish) 2014. http://www.porvoonenergia.fi/fi/hinnastot/toistaiseksivoimassaolevatsahkosopimukset (accessed July 1, 2014).

[69] Tampereen Sähkölaitos. Electricity taxation tightened 1.1.2014 (in Finnish) 2014. https://www.tampereensahkolaitos.fi/yritysjaymparisto/ajankohtaista/Sivut/Sahkovero-kiristyi-1.1.2014.aspx (accessed July 1, 2014).

[70] Fortum. Fortum Lähisähkösopimus (self-produced electricity contract) prices (in Finnish) 2014. http://www.fortum.com/countries/fi/yksityisasiakkaat/energiansaasto/sahkon-pientuotanto/hinnastot/pages/default.aspx (accessed July 1, 2014).

[71] Hämäläinen M, Porvoon Energia. Personal communication 2014.

[72] Faninger-Lund H, Lund P. Integration of building and solar energy systems into one predesign tool. Proc. Eurosun '98, Portoroz, Slovenia: 1998.

[73] Lund P, Faninger-Lund H. ALLSOL - Ein integratives Simulationsprogramm für Energiesysteme in Gebäuden. Proc. Gleisd. Sol. '98, Gleisdorf, Austria: 1998.

[74] Laitinen A, Shemeikka J. RET - Single-family house definition (in Finnish). Espoo: 2005.

[75] Knight I, Kreutzer N, Manning M, Swinton M, Ribberink H. European and Canadian non-HVAC Electric and DHW Load Profiles for Use in Simulating the Performance of Residential Cogeneration Systems. vol. 6. 2007.

[76] Jalonen O. The Role of Residential Households as Enablers for Demand Flexibility within an Electric Grid. Master's thesis. Aalto University, 2014.

[77] Fortum. Fortum Aurinkopaketti (PV installation) (in Finnish) 2015. http://www.fortum.com/countries/fi/energiansaasto-ja-ratkaisut/aurinkopaneelit-aurinkopaketti/pages/default.aspx (accessed June 25, 2015).

[78] Motiva. Heat from your own ground - Ground source heat pumps (in Finnish). 2012.

[79] NIBE Energy Systems Oy n.d. http://www.nibe.fi/ (accessed May 11, 2015).

Supplementary Information
Optimal and rule-based control strategies for energy flexibility in buildings with PV

Jyri Salpakari*, Peter Lund
Department of Applied Physics, School of Science, Aalto University
P.O.Box 14100, FI-00076 AALTO (Espoo), Finland
* Corresponding author, tel. +358 50 433 1262, email: jyri.salpakari@aalto.fi

This supplementary information contains detailed descriptions of the models and the appliance run identification algorithm used in this study.

S1. Model for the heating system

The modeled heating system consists of a ground-source heat pump (GSHP) with an auxiliary electric heater, a water tank as thermal energy storage (TES), and a hydronic system for space heating. In addition, domestic hot water (DHW) is heated with a heat exchanger in the TES and an auxiliary electric water heater in the fixed condensing mode, or with the GSHP and a heat exchanger in a DHW storage in variable condensing mode. In variable condensing, GSHP heating is alternated between space heating and DHW heating with a three-way valve to optimize the coefficient of performance (COP) of the heat pump; in fixed condensing, the GSHP is connected to space heating. See Fig. 2 in the main text for a graphical depiction of the system.

S1.1. Ground source heat pump

The temperature dependency of the coefficient of performance (COP) of the GSHP is modeled with the COP of a corresponding ideal Carnot heat pump cycle, with the Carnot efficiency parameter η_{Ca} to account for cycle nonideality, and temperature differences δT_E and δT_C due to heat exchangers [1–3]:

$$COP(T_C, T_E) = \eta_{Ca} \frac{T_E - \delta T_E}{T_C + \delta T_C - (T_E - \delta T_E)} + 1, \quad \text{(S1)}$$

with η_{Ca} = 0.55 [2] and δT_E = δT_C= 5 °C [3]. In addition, the output temperature of the GSHP is limited to $T_{C,max}$= 65 °C, corresponding to currently available commercial devices [4–6]. A minimum time step of Δt_{min} = 10 min is used to model steady-state operation of the GSHP, on the basis that a GSHP takes several minutes to stabilize to steady-state operation after start of the compressor [7]. A constant T_E = 1 °C is used, approximately corresponding to the yearly average obtained from a typical 150 m deep borehole in Finland [8].

The heat pump heats water pumped from the storage tank to temperature T_C:

$$\dot{m} c_P (T_C - T_S) = P_{comp} COP(T_C, T_E). \quad \text{(S2)}$$

An electric heater functions as an auxiliary heat source after the heat pump, with maximum output temperature $T_{H,max}$= 95 °C:

$$\dot{m} c_P (T_H - T_C) = P_{heater}. \quad \text{(S3)}$$

S1.2. Water storage tank

The water tank is modeled as fully mixed with a 1-node model [9,10]. Stratification modeled with multiple nodes could improve the performance of the modeled TES through better preservation of the temperature required for DHW and space heating loads, obtained from the heat pump with decreasing temperature dependency in COP. However, a fully mixed storage model is employed here for reasonable computation times with the dynamic programming (DP) algorithm, which suffers from the well-known curse of dimensionality [11]. The following state equation for the storage temperature is obtained:

$$\begin{aligned} m_S \frac{dT_S}{dt} = \frac{U_{tb} A_{tb} + U_s A_s}{c_P} (T_a - T_S) + \dot{m}_C (T_H - T_S) \\ + \dot{m}_{L,S} (T_R - T_S) - \dot{m}_{DHW,HE} \varepsilon_{HE} (T_S - T_{CW}). \end{aligned} \quad \text{(S4)}$$

Water density and specific heat are assumed constant, with values ρ = 1000 kgm^{-3} and c_P = 4.2 kJkg^{-1}K^{-1}. The insulation U values for the side U_s (0.3-0.4 W m^{-2}K^{-1}, depending on TES size) and top and bottom U_{tb} (0.3 W m^{-2}K^{-1}) of the storage, modeled as a cylinder, were calculated with equivalent thermal circuits [12] for steel walls and 10 cm polyurethane insulation, the heat conductivities of which were obtained from [12,13], and the convection heat transfer

coefficients of water (forced convection, 50 $Wm^{-2}K^{-1}$) and air (free convection, 5 $Wm^{-2}K^{-1}$) obtained from [12]. The heat transfer can be modeled in steady state as the heat capacity of the wall is small. Radiative heat transfer at the surface was neglected. The heat loss from the tank is decoupled from the inside air temperature of the building; this corresponds to the tank situated in e.g. a basement with the heat loss not being well distributed in the dwelling. A constant T_a = 21 °C for the surroundings of the TES is assumed.

The stability condition for the 1-node model is given in terms of the Courant number [14]:

$$Co = \frac{\dot{m}_{max}}{m_S} \Delta t_{TES} \leq 1. \tag{S5}$$

The maximum mass flow $\dot{m}_{max}$ is set to 0.5 kg/s, approximately corresponding to a currently available commercial device [6], and a corresponding integration time step $\Delta t_{TES} \in [\Delta t_{min}, 1\text{ h}]$ is used for the TES model in the simulations.

Validation of the modeling approach in terms of stratification is conducted with an empirical formula for the minimum number of nodes to achieve satisfactory validity [10]. The formula depends on flow conditions characterized by the daily number of turnovers T, and hence approximately matches the mixing due to numerical diffusion with too few nodes [15] to physical mixing due to the flows. For fixed inlets [10]

$$N_{fixed} = 45.8T^{-1.218}, \tag{S6}$$

where the daily number of turnovers is

$$T = \frac{1}{m_s} \int_{day} (\dot{m}_c + \dot{m}_{L,S})\, dt. \tag{S7}$$

In the 3-kWp PV case, empirical minimum number of nodes is 1 in all studied cases for 0.3 m^3 TES. With the larger storage, it is 1 for rule-based controls; for cost-optimal control, its mean value is 1 and maximum 3. Hence, the fully mixed storage model is sufficient in this case except in some parts of the optimal control simulations with 1 m^3 TES.

In the 9-kWp PV case with a medium-temperature heating system, mean minimum number of nodes is 1 for rule-based control and 1-3 for cost-optimal control for the lower end of TES sizes (0.3 m^3, 1 m^3); for the larger storages, the number ranges 1-4 for rule-based controls and 3-6 and above for optimal control. Improved TES performance through stratification could thus be expected in this case especially at the high end of TES sizes.

With a 9-kWp PV system, low-temperature heating system and variable condensing, the mean value of minimum number of nodes is 1–2 for rule-based control; for cost-optimal control it is 3–5. Maximum values are higher. Some improvement due to stratification could hence be expected.

Several technologies to improve stratification in water tanks have been developed, such as inlet diffusers and baffle plates [16]. These were not employed in the measurements that were used to devise the aforementioned validation formula [10,17]. However, to the best of the authors' knowledge, an experimentally validated dynamic system model suitable for optimal control studies to account for these devices has not been presented.

S1.3. Hydronic heating system

The time constant of radiators is approx. 0.5 h [18], fast enough to neglect their dynamics in hourly energy balance. The integration time steps (Eq. (S5)) can be shorter than 0.5 h; the effect of radiator dynamics on the hourly temperature and mass flow values is considered small and neglected. Depending on how it is laid out, floor heating may have significantly larger thermal inertia [18,19] and this model may hence not be directly applicable to it. The thermal dynamics of water in the heating system when it is inactive [19] is neglected. Hence, heat transfer from the water in the hydronic system to the dwelling space is modeled simply as

$$P_{SH} = \dot{m}_L c_P (T_I - T_R). \tag{S8}$$

The input temperature of the radiators T_I is controlled by the shunt valve depending on outdoor temperature T_O according to a given control curve, resulting in the mass flow from and to the storage

$$\dot{m}_{L,S} = \frac{T_I - T_R}{T_S - T_R} \dot{m}_L. \quad \text{(S9)}$$

The control curves of a medium and low-temperature heating system in Table 1 are used. Constant return temperatures T_R = 30 °C and T_R = 25 °C are assumed, respectively. This corresponds to inverter-controlled circulation pumps.

Table S1. Heating system control curves.

T_O (°C)	$T_{I,m}$ (°C)	$T_{I,l}$ (°C)
-26	60	40
5	40	30
30	40	30

S1.4. Domestic hot water

The domestic hot water heat exchanger in the storage tank is modeled with a constant effectiveness heat exchanger model

$$T_{DHW,HE} = T_{CW} + \epsilon_{HE}(T_S - T_{CW}), \quad \text{(S10)}$$

with ε_{HE} = 0.9. As the model is designed for use with hourly DHW consumption data, more sophisticated heat exchanger models with dependency on instantaneous mass flow are not applicable. A constant cold water temperature T_{CW} = 6 °C is assumed in the Finnish case study in this paper.

A constant set point T_{DHW} = 55 °C is used in this work, in compliance with Finnish building code [20]. In fixed condensing heat pump operating mode, the DHW storage is controlled to keep this temperature with an electric heater and is large enough to provide hourly consumption (maximum approx. 50 l in the case study in this paper). In this size scale, its losses are negligible. The tank averages DHW heater power over the hourly time step.

In variable condensing mode, DHW is heated to the setpoint with the GSHP and a heat exchanger in the DHW storage. Typical size for a DHW storage in this setup is 200 l [21], the losses of which are negligible. A temperature drop δT_{DHW} = 5 °C is assumed in the heat exchanger in the DHW storage, resulting in the following compressor power required for DHW heating:

$$P_{comp,DHW} = \frac{\dot{m}_{DHW} c_P (T_{DHW} - T_{DHW,HE})}{COP(T_{DHW} + \delta T_{DHW}, T_E)}. \quad \text{(S11)}$$

S1.5. Variable condensing

Variation between space heating (SH) and DHW with the GSHP in variable condensing mode is modeled inside the hourly time step. The hourly average compressor power is

$$P_{comp} = P_{comp,SH} + P_{comp,DHW}. \quad \text{(S12)}$$

Shares of the time step required to deliver these hourly averages, along with hourly average P_{heater}, are solved. The system is integrated with corresponding instantaneous powers and integration time steps Δt_{SH}, $\Delta t_{DHW} \in [\Delta t_{min}, \Delta t_{TES}]$. DHW and TES heating take turns until either one is delivered, after which the remaining one is finished. In the variable condensing case, the modeled heat pump has to be inverter controlled as the instantaneous power varies depending on the time step division to TES and DHW heating.

S2. Model for the electrical system

The flexibility electrical energy system in the model comprises shiftable appliances and a battery.

S1.6. Shiftable electrical appliances

Shiftable appliances are modeled with an average $n_{hours,shiftable}$-hour demand cycle representing all the shiftable appliances in the building to simplify the model in order to keep computation times for optimal control reasonable. The model requires as input data the $n_{hours,shiftable}$-hour demand cycle, the original appliance starting times and the number of shiftable appliances $n_{shiftable}$.

The following discrete state equation, compatible with the DP algorithm, counts the number of shiftable runs in the system model:

$$l_{k+1} = l_k + r_k, \tag{S13}$$

where l_k is the log of performed runs and r_k is the number of runs started in the simulation at time step *k*. Shifting of the appliance runs is allowed during each day between midnights.

S1.7. Battery

The Li-ion battery is modeled with a simple storage model to limit the number of dimensions in the optimal control problem. The energy content of the battery is

$$E_{battery,k+1} = E_{battery,k} + P_{battery,k}\Delta t, \tag{S14}$$

and for the system comprising the battery and bidirectional inverter,

$$P_{battery,syst} = \begin{cases} \dfrac{1}{\eta_{inverter}} P_{battery}, & P_{battery} \geq 0, \\ \eta_{inverter}\eta_{battery} P_{battery}, & \text{otherwise.} \end{cases} \tag{S15}$$

80% of the nominal capacity is used for increased cycle life. In the corresponding capacity range 10–90%, the used linear model is a good approximation. Battery aging is not considered in the model. Constant values $\eta_{battery} = 0.95$ [22] and $\eta_{inverter} = 0.9$ [23] are used. Self-discharge of Li-ion batteries is only 3–5% per month [24], thus negligible compared to the cycle efficiency as the battery is used relatively often in the considered control strategies.

S3. Shiftable appliance identification algorithm

The simple algorithm decribed below was used for identifying shiftable appliance runs in this work. It is based on the observation that in all but one of the measured cases, a run of a shiftable appliance occurred when the total consumption was at least 900 W in excess of the base load.

1. For all hours of the year, find the base load as the minimum consumption of the 25 hours centered at the hour. Label the hour as containing shiftable load if the power is over baseload + 900 W.
2. Find the hour of peak power of the intervals labeled as containing shiftable load, by finding the time when the sign of power difference to the previous hour changes from positive to negative. Label each peak as start of a shiftable 3-hour demand cycle.
3. In decreasing order of magnitude of the peaks, add additional cycle until the total electricity consumption of the appliances over the year corresponds to total yearly consumption of the appliances. The time period in which the shiftable appliances were measured is assumed representative of their use over the year.

Figures 1 and 2 show the results achieved with this algorithm in the time periods with measured appliance-level data. The algorithm results in only one false negative. 4 false positives are identified in the washing machine and tumbler time series and 12 in the dishwasher time series. False positives are expected as the appliances were not measured simultaneously. The 12 false positives in the 211-h dishwasher time series correspond approximately to the 10 measured runs in the 192-h washing machine and tumbler series. Similarly, the 4 false positives in the washing machine and tumbler series correspond approximately to the 3 runs in the dishwasher time series; as only one of the two dishwashers in the house was measured, more dishwasher runs are expected to have occurred.

It can be concluded that the simple algorithm performs reasonably well. Throughout the year, the algorithm identifies four coincidental shiftable runs at maximum, hence not exceeding the number of four shiftable appliances available in the house.

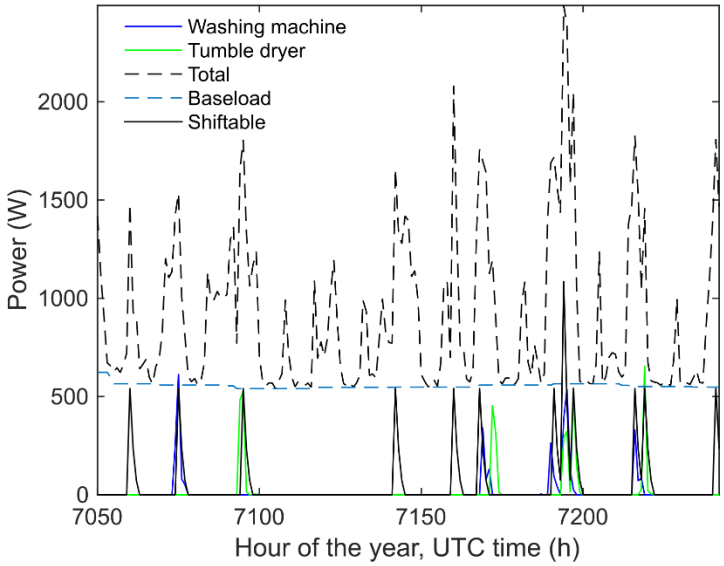

Figure S1. The modeled shiftable loads with measured washing machine and tumbler loads.

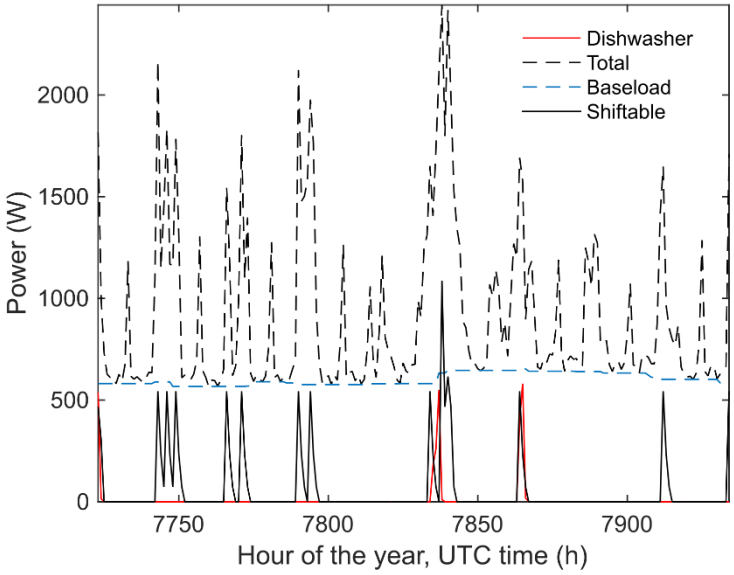

Figure S2. The modeled shiftable loads with measured dishwasher load.

References

[1] Forsström J, Lund P. Optimization of operating strategies in a community solar heating system. Appl Math Model 1985;9:117–24.

[2] Wikstén R. Thermodynamic processes (in Finnish). 4th ed. Helsinki: Helsinki University Press; 2009.

[3] Sullivan HF. Principles of Vapour Compression Heat Pumps. In: Berghmans J, editor. Heat Pump Fundam., The Hague: Martinus Nijhoff Publishers; 1983, p. 14–33.

[4] NIBE F1345 2014. http://www.nibe.fi/Tuotteet/Maalampopumput/Tuotevalikoima/F1345/ (accessed June 27, 2014).

[5] IVT Greenline HE 2014. http://www.ivt.fi/pages/product.asp?lngID=204&lngLangID=1 (accessed June 27, 2014).

[6] NIBE F1155 2014. http://www.nibe.fi/Tuotteet/Maalampopumput/Tuotevalikoima/NIBE-F1155/ (accessed June 27, 2014).

[7] SENERA Oy. Ground heat (in Finnish) 2015. http://www.senera.fi/Maalampo/ (accessed May 25, 2015).

[8] Leppäharju N. Geophysical and geological factors affecting the use of bedrock heat (in Finnish). Master's thesis. University of Oulu, 2008.

[9] Duffie J, Beckman W. Solar Engineering of Thermal Processes. 4th ed. John Wiley & Sons; 2013.

[10] Kleinbach EM, Beckman WA, Klein SA. Performance study of one-dimensional models for stratified thermal storage tanks. Sol Energy 1993;50:155–66.

[11] Bertsekas DP. Dynamic Programming and Optimal Control, Volume I. 3rd ed. Belmont, Massachusetts: Athena Scientific; 2005.

[12] Incropera FP, DeWitt DP. Fundamentals of Heat and Mass Transfer. 2nd ed. John Wiley & Sons; 1985.

[13] Wu J-W, Sung W-F, Chu H-S. Thermal conductivity of polyurethane foams. Int J Heat Mass Transf 1999;42:2211–7.

[14] Arias D, McMahan A, Klein S. Sensitivity of long-term performance simulations of solar energy systems to the degree of stratification in the thermal storage unit. Int J Energy Res 2008;32:242–54.

[15] Powell KM, Edgar TF. An adaptive-grid model for dynamic simulation of thermocline thermal energy storage systems. Energy Convers Manag 2013;76:865–73.

[16] Han YM, Wang RZ, Dai YJ. Thermal stratification within the water tank. Renew Sustain Energy Rev 2009;13:1014–26.

[17] Kleinbach EM. Performance Study of One-Dimensional Models for Stratified Thermal Storage Tank. Master's thesis. University of Wisconsin-Madison, 1990.

[18] Karlsson F, Fahlén P. Impact of design and thermal inertia on the energy saving potential of capacity controlled heat pump heating systems. Int J Refrig 2008;31:1094–103.

[19] Good N, Zhang L, Navarro-Espinosa A, Mancarella P. High resolution modelling of multi-energy domestic demand profiles. Appl Energy 2015;137:193–210.

[20] Ministry of the Environment. The National Building Code of Finland. D1 Water supply and drainage installations for buildings (in Finnish). Finland: 2007.

[21] NIBE Energy Systems Oy n.d. http://www.nibe.fi/ (accessed May 11, 2015).

[22] Reddy TB. An Introduction to Secondary Batteries. In: Reddy TB, Linden D, editors. Linden's Handb. Batter. 4th ed., McGraw-Hill; 2011.

[23] Riffonneau Y, Bacha S, Barruel F, Ploix S. Optimal Power Flow Management for Grid Connected PV Systems With Batteries. IEEE Trans Sustain Energy 2011;2:309–20.

[24] Lu L, Han X, Li J, Hua J, Ouyang M. A review on the key issues for lithium-ion battery management in electric vehicles. J Power Sources 2013;226:272–88.